JOURNAL OF THERMOPHYSICS AND HEAT TRANSFER
Vol. 8, No. 3, July–Sept. 1994

Analysis of the Argon Additive Influence on a Nitrogen Arcjet Flow

A. T. Schönemann,* M. Auweter-Kurtz,† H. A. Habiger,* P. C. Sleziona,‡ and T. Stöckle§
Institut für Raumfahrtsysteme, University of Stuttgart, 70550 Stuttgart, Germany

Two plasma wind tunnels for the simulation of conditions encountered by space vehicles during planetary entry, and for the development and qualification of heat protection material, are in use at the Institute for Space Systems. The plasma is produced by a magnetoplasmadynamic (MPD) accelerator, specially designed for the use of gas mixtures such as N_2/O_2 and carbon containing gas mixtures. At high mass flow rates and low power levels a protective gas layer of argon is produced at the anode for a N_2/O_2 flow. The influence of the Ar additive on a nitrogen plasma is investigated experimentally by means of electrostatic probes, mass spectrometry, pitot probes, and heat flux probes; and numerically with a program especially developed for the simulation of the high enthalpy flowfield of MPD accelerators. The existing numerical code for solving the chemical reactions within an air plasma was extended by argon/air reactions. A comparison between the experimental data set and the numerical simulation of the plasma flow is made for a N_2 and a N_2/Ar plasma.

Introduction

TWO plasma wind tunnels[1,2] were built at the Institut für Raumfahrtsysteme (IRS) of the University of Stuttgart for the simulation of re-entry or entry conditions with high specific enthalpies and low pressures as required for the development of modern oxidation protected materials for the thermal protection of spacecraft.[3] The wind tunnels are connected to a power supply of 6 MW and a roots pump vacuum system with a total suction power of more than 250,000 m^3/h. The wind tunnels are equipped with a continuously operating magnetoplasmadynamic (MPD) accelerator, designed for power levels up to 0.5 MW and for specific enthalpies ranging from 5 MJ/kg up to more than 150 MJ/kg. The stagnation pressure reaches from 0.1 up to 50 mbar. The maximum mass flow rate is at the moment about 30 g/s.

The MPD accelerator RD5 used in PWK2 for experimental investigations is shown in Fig. 1. Inert gases like N_2, H_2, and Ar can be fed in along the cathode, which is made of thoriated tungsten and is in a glowing state during operation, giving a very low cathode erosion rate, while oxidizing and carbon containing gases like O_2 or CH_4 are inserted with high radial velocity just behind the nozzle throat. The anode, the neutral segments of the nozzle, and the cathode support are all water cooled.

At high mass flow rates and low power levels the current attachment at the anode tends to be no longer diffuse with a N_2/O_2 plasma flow, due to a decrease of ions in the anode sheath. Therefore, at the anode a rare gas layer of argon, which can be easily ionized, is produced by tangential injection. The argon additive is essential for providing a stable arcjet flow over several hours, and also for avoiding erosion due to an onset of the arc at the anode, i.e., with argon additive there is no copper and no cathode erosion material[4] in the plasma jet.

Different well known experimental methods are applicable for the investigation of the plasma conditions.[3,5–7] All probes are mounted on a platform with four motor driven axes. Three of these axes are linearly oriented, the fourth one provides the possibility to rotate the probes. The moving range of the platform is about 900 mm in x direction, i.e., distance to the anode, 400 mm in y direction, i.e., perpendicular to the plasma jet axis, and about ± 75 mm in z direction, i.e., vertical shift to the centerline. Due to its dimensions, the mass spectrometer is only movable in x and y directions. The frame of references (x, y, z) is shown schematically in Fig. 3.

Experimental Investigations

The chosen conditions are an ambient pressure of 1.3 mbar, a current of 1000 A, a mass flow rate of 1.0 g/s N_2 and, in case of the N_2/Ar plasma, an additional mass flow rate of 0.3 g/s Ar as anode protection gas. This leads to an average specific enthalpy at the end of the anode of about 30 MJ/kg. Radial distributions of the pitot pressure, the local heat flux, the electron temperature, the electron density, and the neutral particle distribution are measured at two different axial positions, x = 260 and 330 mm for each plasma. Additionally,

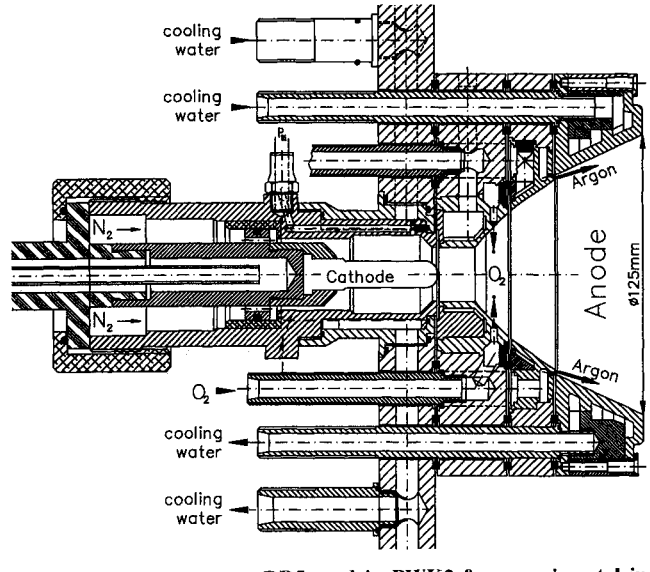

Fig. 1 Plasma generator RD5 used in PWK2 for experimental investigations.

Presented as Paper 93-2829 at the AIAA 28th Thermophysics Conference, Orlando, FL, July 6–9, 1993; received July 12, 1993; revision received Oct. 26, 1993; accepted for publication Nov. 5, 1993.

*Diplom-Physiker, Scientist, Wind Tunnel Experiments. Member AIAA.
†Professor, Aerospace Engineering. Member AIAA.
‡Doktor-Ingenieur, Numerical Simulation.
§Diplom-Ingenieur, Numerical Simulation.

the plasma velocity and the ion composition are measured at a few discrete points in the plasma jet.

The mass flow rate of argon is normally about 5% of the total mass flow rate. To increase possible effects of the argon on the N_2 plasma, a higher amount, ca. 30%, of the argon additive is used for these investigations.

The conditions were chosen so that 1) a destruction of the probes due to harsh environmental conditions of the plasma can be avoided, 2) pressures are high enough to be simulated within a Navier-Stokes program, and 3) pressures are low enough so that the mass spectrometer can be used to gain a reliable particle distribution within the plasma.

To determine the composition of the plasma flow and the distribution of neutral particles and ions in the plasma jet, mass spectrometry is used.[8] The mass spectrometer consists of a quadrupole mass filter, a cylindrical mirror energy analyzer, an ion source, and a channeltron. Therefore, mass and energy analysis of neutrals as well as positive and negative ions is possible.[9] The spectrometer's outer front dimensions are similar to those of material probes used for material tests in the plasma wind tunnel (PWK). It is originally used to measure the plasma conditions in a stagnation point in front of a material sample. The plane orifice serves for sampling plasma particles into the spectrometer and provides for one-staged differential pumping. It is made of tungsten with opening diameters of 100 μm down to 10 μm. The electronics are situated 32 mm behind the opening inlet, thus avoiding recombination due to long paths inside the measurement device. By means of a plasmaphysical model describing the space charge sheath in front of a plane probe inside a plasma,[10,11] it is possible to estimate the electron temperature and charged particle density in front of the orifice.

A correction factor due to the dimension ratio length/diameter of the orifice is applied to the measured data.[12] Additionally, the increase of pressure inside the mass spectrometer due to the high stagnation pressure in front of the orifice is taken into account for the correction of the measured data. The accuracy of the measurements is limited mainly by the correction factors concerning the stagnation pressure and the dimension ratio factor, because here the effects of recombination in front of the orifice are included. It is shown later that the error is about 20% in the center of the plasma jet. The high system pressure inside the mass spectrometer with a 100 μm orifice when it is placed into the center region of the plasma jet prevents the measurement of a radial distribution of the external ions. So, external ions were detected only at a few points in the plasma jet to determine what kinds of ions at what energies will occur.

Figures 2 and 3 depict as an example the radial distributions of neutral particles at x = 260 mm for both cases. The diagrams show the corrected count rates, but the part of ionized

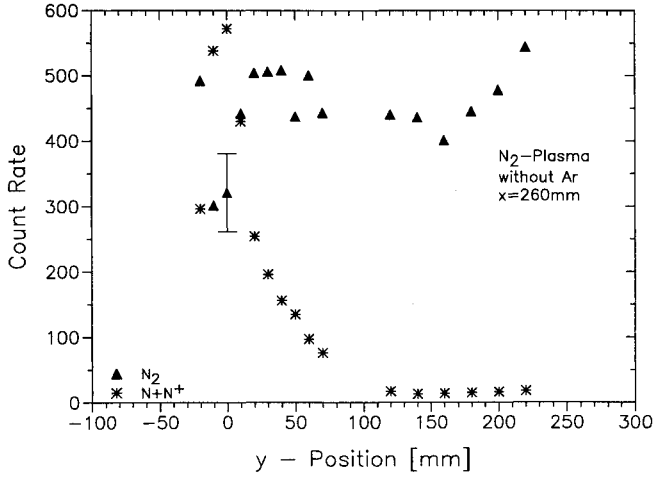

Fig. 2 Neutral particle distribution at x = 260 mm in a N_2-plasma.

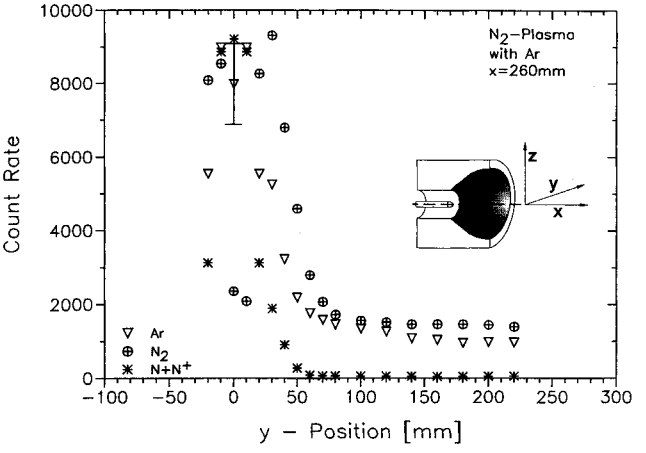

Fig. 3 Neutral particle distribution at x = 260 mm in a N_2/Ar-plasma.

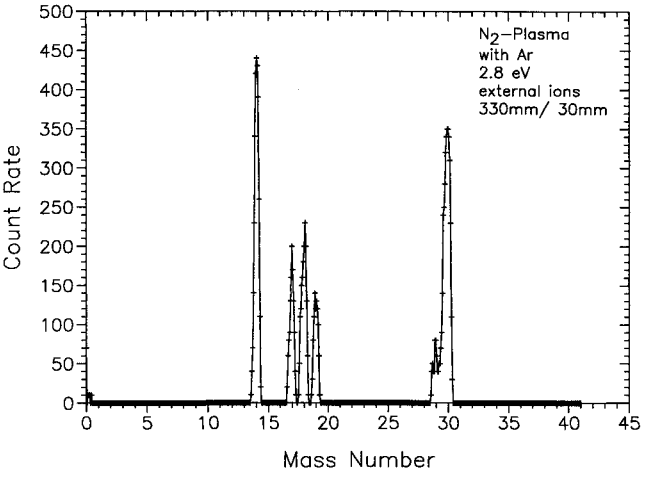

Fig. 4 Mass spectra of external ions (N^+, OH^+, H_2O^+, H_3O^+, NO^+) in a N_2/Ar-plasma at x = 330 and y = 30 mm.

nitrogen atoms which recombined in front of or inside the orifice is still included in the neutral nitrogen atom count rate. Since the total count rate at each point in the distribution (sum of all particle count rates) should be nearly constant, the corrected data obviously have an error of some percent (especially for N_2/Ar).

Figure 4 shows a mass spectra of external ions in a N_2/Ar-plasma at x = 330 mm, y = 30 mm, and an energy of 2.8 eV. The mass peak at m = 14 is typically a N^+ signal. Mass peaks at 17, 18, and 19 amu are due to water molecules of the ambient gas in the wind tunnel which were ionized in front of the orifice. Ions at m = 30 are NO^+-ions which are also produced in front of the orifice. Ar^+-ions at m = 40 are not detected. Thus, only atomic nitrogen ions are produced in the plasma freestream. Taking the measured ion energy of 2.8 eV and the orifice floating potential of 1.2 V, an ion temperature of 4579 K can be calculated for this position in the plasma jet.

The measured count rates are converted into partial pressures for further use by assuming a constant static pressure over the whole plasma jet which is equated to the sum of the count rates.

Electrostatic probes[13] are used to determine the electron temperature, density, and the plasma velocity. An electrostatic probe consists of a cylindrical tungsten electrode, which is placed inside a plasma and aligned with the plasma streamlines, while its dimensions are matched with the plasma conditions such as the Debye length and the mean free path of the ions. This method is applied to obtain a voltage-current characteristic for different types of probes such as single, double,[14] and triple[15] probes. The measurements have been car-

ried out with all these different types of probes to improve the reliability of the results. The accuracy of the measurements depends on the kind of probe used, the pressure, and the probe's distance to the anode. The estimated error is 10–20% for a double probe.

For the determination of the plasma velocity, two double probes are separated at a known distance and aligned with the plasma flow to determine the plasma velocity by the detection of the time of flight of local ion density fluctuations.[16] Measurements are most reliable in the center of the plasma jet where the plasma streamlines can be assumed to be parallel.

In Fig. 5 the electron temperature measured with double probes in the N_2- and the N_2/Ar-plasma at x = 260 mm is shown. The temperature is slightly higher in a pure N_2-plasma and its slope has a flatter shape.

In Fig. 6 the electron density measured with double probes is shown for both plasmas. Here, the density is slightly higher for the N_2/Ar-plasma.

The velocity distribution is measured by time of flight probes in the center region of the plasma jet. Additionally, it was calculated with the total pressure and iteratively determined by the calculation of the local specific enthalpy and mole fractions (cf. next chapter). In Fig. 7 all distributions are shown for the N_2-plasma at x = 260 mm. The velocity distribution which was determined by the local specific enthalpy was used for the numerical simulation. In case of argon added, the values of the velocity are lowered by about 10%.

The dynamic or stagnation pressure of the plasma jet is measured with a pitot probe. The probe used here has a geometry identical to the material support system used for

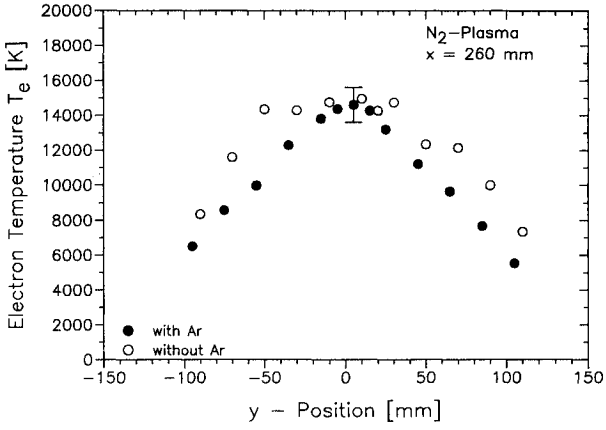

Fig. 5 Electron temperature distribution in a N_2 and N_2/Ar-plasma at x = 260 mm.

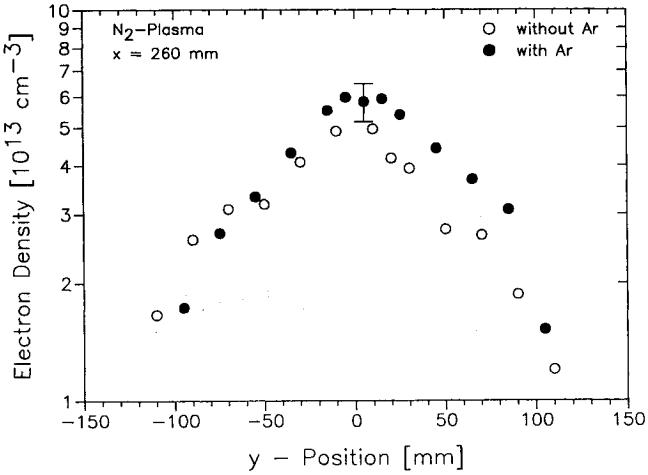

Fig. 6 Electron density distribution in a N_2 and N_2/Ar-plasma at x = 260 mm.

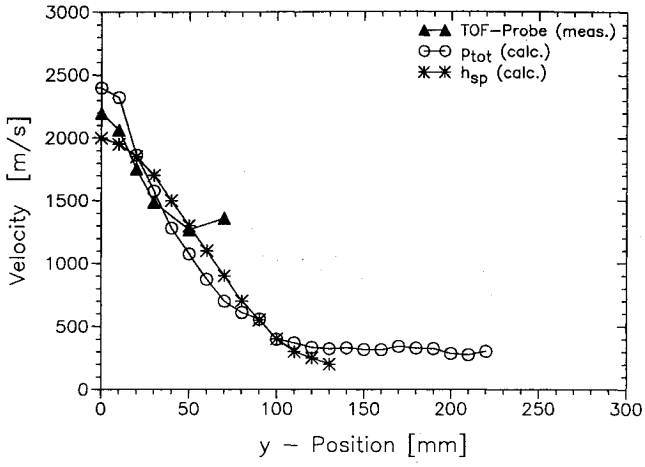

Fig. 7 Measured and calculated velocity distributions in a N_2-plasma.

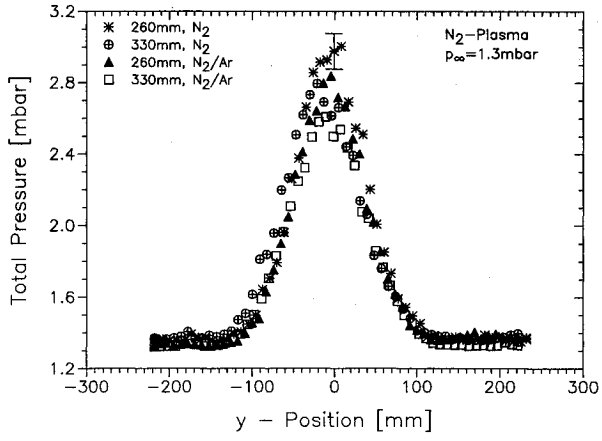

Fig. 8 Total pressure distribution at x = 260 and 330 mm for both plasmas.

material tests. It is a cylindrical-shaped, water cooled copper probe with an o.d. of 50 mm and an opening inlet of 17 mm in diam. The front face edges are rounded to an aerodynamical form.

The accuracy of the pressure measurement is estimated to be within 5% with respect to fluctuations of the vacuum system and of the plasma jet, deviations in reproducing the test conditions, and the accuracy of the pressure gauge.

In Fig. 8 the total pressure distributions are shown. The total pressure, i.e., the dynamic pressure, is clearly decreased by around 0.2 mbar in case of argon added at the MPD accelerator.

The heat flux is measured by a stationary heat flux probe. It is a calorimetric probe which is geometrically similar to the pitot probe. The actual probe is an insert into the front plate of the water cooled copper device and consists of a water cooled copper tube. The insert is thermally insulated with a ceramic inlay from the surrounding support. The heat flux to the probe is determined by the front side area of the insert, the water flow rate, the temperature difference between incoming and outgoing water, and the heat capacity of water.

The accuracy of the method is given by the deviation of the thermocouples used for detection of the temperatures and by the accuracy of the water flow meter. Of course, effects of dissociation, ionization, and catalytic reactions in front of and at the wall of the insert will affect the measured heat flux. Since the insert is made of copper the detected heat flux is not the fully catalytic heat flux. The accuracy of the heat flux measurements is about 10%.

The measured heat fluxes at the different positions in the nitrogen and nitrogen/air plasma are shown in Fig. 9. The

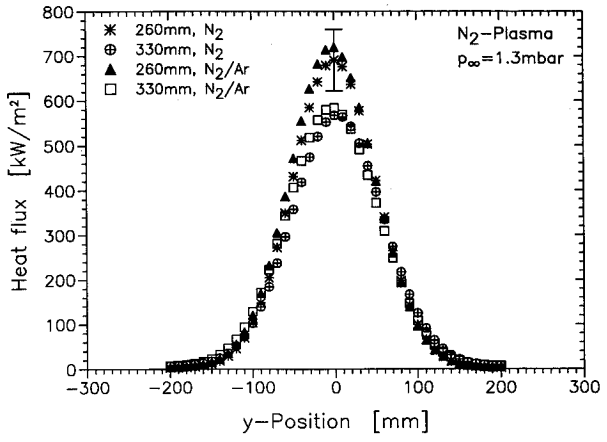

Fig. 9 Stationary heat flux distribution at x = 260 and 330 mm for both plasmas.

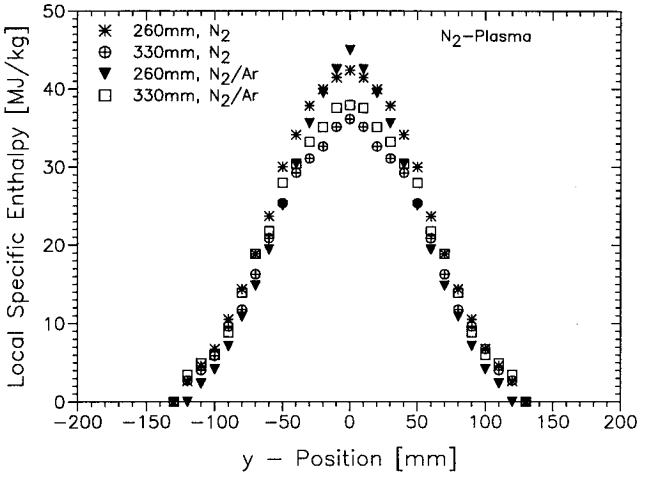

Fig. 10 Calculated local specific enthalpy for both plasmas.

heat flux to the probe is slightly higher in case of argon added to the plasma (ca. 3–4%).

Using the measured heat flux, the surface temperature of a material sample exposed to these plasmas with an emissivity of 0.8 (e.g., SiC) can be estimated by the Stefan-Boltzmann law. The calculated temperatures are 1982 K (N_2) and 1995 K (N_2/Ar), thus, only a small temperature difference of 10 K is expected. Of course, the real surface temperature of the material may be lower than the calculated temperature due to the lower heat flux to the low catalytic SiC.

Determination of the Local Specific Enthalpy and Mole Fractions

Any fluid in motion at high temperatures is characterized by the specific enthalpy which contains the kinetic energy and the chemical energy of the flow, i.e., heat transfer, velocity, dissociation, ionization, and formation energies. A method to investigate the local specific enthalpy in the freestream plasma flow is given by the theory of heat transfer by Pope,[17–19] where the enthalpy can be calculated with the local total pressure and the heat flux. The theory also takes into account that the copper surface of the heat flux probe cannot be assumed to be fully catalytic. Thus, the measured non-catalytic heat flux is corrected by a factor which itself strongly depends on the local specific enthalpy. The enthalpy distributions obtained with this theory are given in Fig. 10. The enthalpy is slightly higher for the argon case.

Knowing the local specific enthalpy, the electron temperature and density, the ambient pressure, and the velocity, the concentrations of the plasma components in case of pure nitrogen can be calculated by the energy equation. The basic assumptions are, a constant static pressure over the whole plasma jet, only singly ionized atomic nitrogen present in the flow, a quasineutrality, i.e., the density of ions equals that of the electrons, a thermal nonequilibrium of electron and ion temperature of $T_e/T_i \approx 2$, and a mixture of ideal gases where the rotational temperature equals the translational and the vibrational temperature equals the electron temperature. The method is given in detail in Refs. 20 and 21.

The mole fractions are calculated for the pure nitrogen case. They again can be compared with the measured particle distribution of the mass spectrometer. Additionally, the above mentioned theory can be extended with argon. Since the mass spectrometric measurements shows no significant amounts of ionized argon, its ionization energy can be neglected in the energy calculation, and the argon has only to be taken into account for the evaluation of the average mole mass, the degrees of freedom (DOF), and the heat capacity. Figure 11 depicts the calculated mole fractions Ψ_N, Ψ_{N_2}, and Ψ_{N^+} for N, N_2, and N^+, and the measured mass spectrometric data at the second cross section for the N_2-plasma. The particle distributions can be said to be qualitatively the same, but

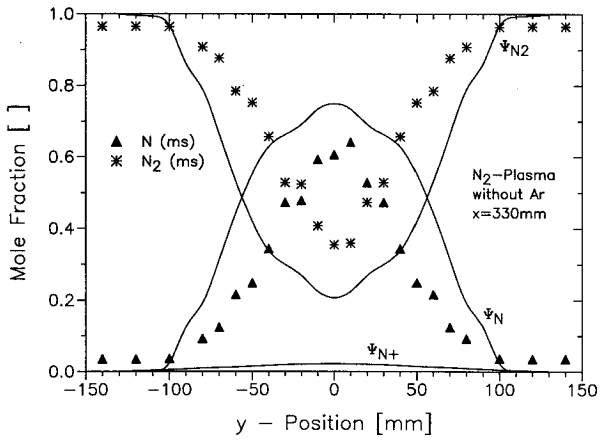

Fig. 11 Calculated mole fractions Ψ_{N_2}, Ψ_{N_1}, Ψ_{N+} and measured mass spectrometric data in a N_2-plasma.

obviously the influence of recombinations in the stagnation point is underestimated when correcting the mass spectrometric data. This leads to a roughly 20% higher amount of molecular nitrogen (and lower amount of atomic nitrogen) in the center of the jet. Taking the measured mole fractions, the local specific enthalpy can be recalculated with 32.15 MJ/kg, i.e., 11% lower than that shown above (see Fig. 10).

To verify the calculations the total pressure can be recalculated by applying the gained data to the Bernoulli equation of compressible flows and comparing the measured and calculated total pressures. This is an iterative process where some of the assumptions are varied. When both pressures are equal, some more results are gained: the thermal nonequilibrium in the center of the plasma jet can be set to $T_e/T_i \approx 1.9$, the Mach number in the center of the jet is ≈0.9, and the velocity is lowered by about 10% of the measured values (cf. Fig. 7).

Numerical Simulation Program

For the numerical investigations, a two-dimensional, axisymmetric program system[22,23] is used consisting of a Navier-Stokes flowfield solver, a solution program for the electron energy equation yielding the electron temperature, and a code for the evaluation of the vibrational energy and the species conservation equations. The flowfield can be calculated for chemical and thermal nonequilibrium.

The numerical model is formulated for air as fluid medium, the governing equations are, total mass conservation, momentum conservation, total energy conservation, species conservation (formulated in molar concentrations), vibrational energy conservation, and electron energy conservation equation. The transport coefficients for the air case are described

by the Yos model.[24] Mass diffusion is implemented in the appropriate equations, while thermal and pressure diffusion have been neglected. The equation system is divided in three parts, which are solved in the following sequence: 1) the flowfield code, 2) the chemical and vibrational energy code, and 3) the electron energy code. For the calculation of the flow, the electron energy, the vibrational energy, the nonequilibrium chemical reactions, and the flowfield codes are correlated by appropriate source terms. For a given flowfield, the electron temperature, and hence, the chemical composition including the vibrational energy equations are determined. With these results the flowfield equations are integrated in the next iteration step. This new flowfield and the new distribution of the electron temperature are taken to calculate the new chemical properties and vibrational temperatures, etc. These sequences are repeated until the calculated values have reached numerical equilibrium. The nonlinear, elliptical partial differential equation of the electron energy conservation is solved with a finite difference method. The discretization yields a nonlinear equation which is iteratively solved with a modified Gauss-Seidel algorithm. The nonlinear, hyperbolic partial differential equation for the flowfield conservation equations is solved with a finite volume method, which was modified for a nonequilibrium state. The species conservation and the vibrational energy equation are solved with an explicit MacCormack predictor-corrector algorithm.[25]

Chemical Model

In the chemical part the Park[26,27] model for air is implemented. The model includes 11 different particles (N, O, N_2, NO, O_2, O^+, N^+, O_2^+, N_2^+, NO^+, e^-) undergoing six different kinds of reactions: dissociation due to impact with a heavy particle or with an electron, exchange reactions, associative ionization, electron impact ionization of atoms, and charge transfer reactions. Thus, 47 reactions with their corresponding reaction rates are included in the model.

This model has to be extended with 15 argon reactions,[28] i.e., dissociation reactions of O_2, N_2, and NO, ionization reactions of O, N, O_2, N_2, and NO due to an Ar or Ar^+-impact, and charge exchange reactions were included.[29-36] Since there was no rate constant found for the recombination reaction of N and O to NO by Ar impact, it is estimated by the function for the backward reaction of the recombination of NO with N of the Park model. There was only an upper limit for the charge exchange reaction between N and Ar^+. Ionization due to impact of an Ar atom was not found in literature. Since impact ionization is effective only at higher energies, the rate constants are assumed to be 1/1000 of the rate constants of charge exchange reactions. Additionally, the electron impact ionization and recombination rates of Ar are determined by a gas kinetic consideration using the Ramsauer cross section,[37]

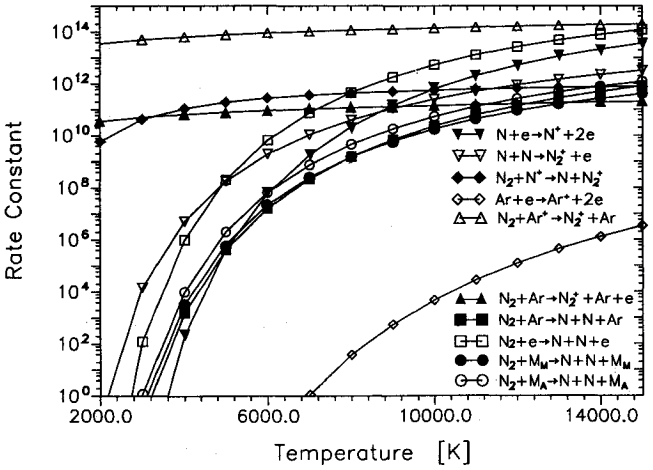

Fig. 12 Rate constants of the forward reactions including Ar.

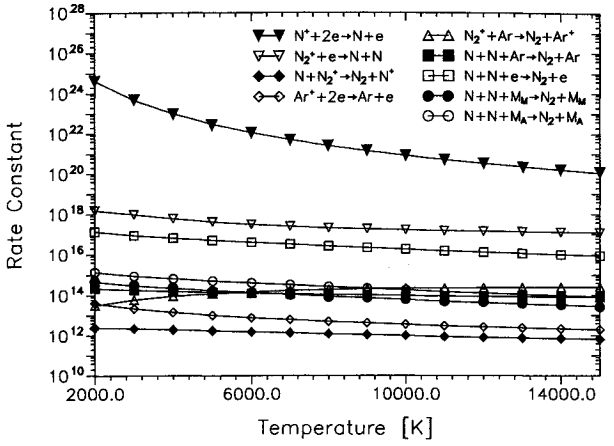

Fig. 13 Rate constants of the backward reactions including Ar.

and the Gvosdover cross section,[38] respectively. The rate constants of the backward and forward reactions are shown in Figs. 12 and 13.

The transport coefficients cannot be calculated within the implemented model of Yos,[24] since it yields no collision integrals for interactions with argon. Therefore, the transport coefficients like dynamic viscosity and heat conductivity of heavy particles—the vibrational and rotational parts—are implemented with a Burhorn[39] model. Here, the coefficients are determined according to the mean free paths of the particles. The diffusion coefficient is calculated with a Schrade[40] model where the diffusion coefficient of one component is related to the cross section of this component with all other particles and diffusion occurs because of a pressure gradient. The diffusion coefficients of the air components are adjusted to the Schrade model by multiplying them by the temperature.

Comparison of the Experimental and Numerical Results

For the numerical simulation of the expansion and development of the plasma freestream flow between the two cross sections, the experimental data set at the first cross section (260 mm) is used as the starting parameter. Then, the data set at the second cross section (330 mm) is calculated and the results are compared with the experimental data set gained here.

Apart from the data shown in the figures above, a few additional assumptions have to be made for the numerical calculations. At first, the static pressure is assumed to be constant throughout the whole plasma jet, i.e., 1.3 mbar. Secondly, the temperature of the heavy particles is set equal to the temperature of the ions, which itself is estimated by the thermal nonequilibrium between electrons and ions of $T_e/T_i \approx 2$ inside the plasma flow. Outside the plasma flow, where no experimental data exist, the data set is completed by an exponentially decreasing function. The measured count rates of the mass spectrometer were converted into partial pressures by taking the static pressure and the electron density as the value for the total particle density.

First, numerical calculations showed a high production rate of electrons at the second cross section in case of the pure N_2-plasma where the calculated electron density increased by a factor of 3 compared to the experiment. Therefore, the experimentally determined electron temperature was reduced by 15%, which is still within the error given for the electrostatic probe measurements. On the other hand, the chemical model used for the simulation is valid up to about 12,000 K. Higher values are extrapolated, and so this extrapolation can induce also the inconsistence in the data set. This effect did not occur in case of the N_2/Ar-plasma.

Figures 14–17 show the comparison between measured and calculated electron, vibrational and heavy particle tempera-

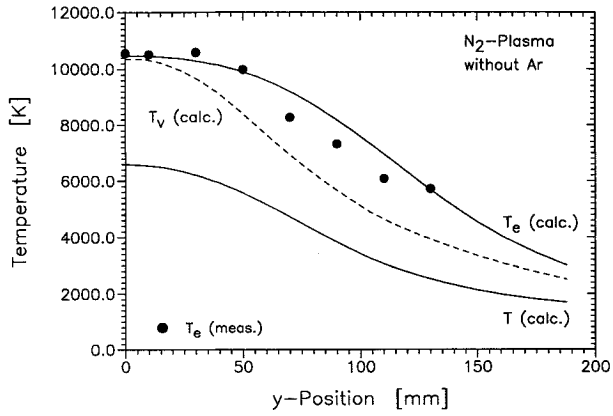

Fig. 14 Comparison of the electron, vibrational, and translational temperature at the second cross section in a N_2-plasma.

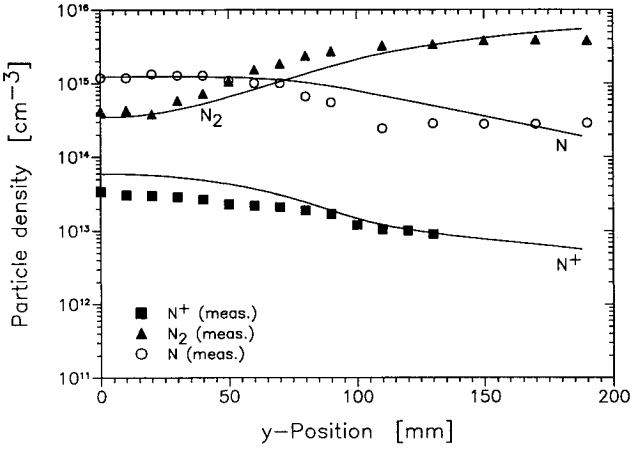

Fig. 15 Comparison of the particle distribution at the second cross section in a N_2-plasma.

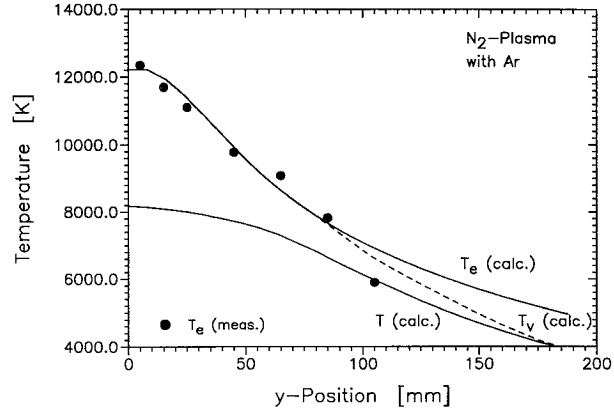

Fig. 16 Comparison of the electron, vibrational, and translational temperature at the second cross section in a N_2/Ar-plasma.

ture, and particle distribution at the second cross section for both plasma flows. The electron temperature compares very well with measured data for the N_2-plasma. The normal assumption of equality between electron and vibrational temperature seems only to be valid in the center of the jet, in the outer parts of the jet the vibrational temperature nearly equals the heavy particle temperature. The particle distribution is simulated qualitatively and quantitatively well for the N_2-plasma, with a N^+ density which is still a little overpredicted as explained above. In case of the N_2/Ar-plasma, the temperature distributions compare very well. For the particle distribution, the experimental and numerical data differ by 30–40% in the center of the jet. These quantitative differences can arise due to 1) the too high calculated vibrational

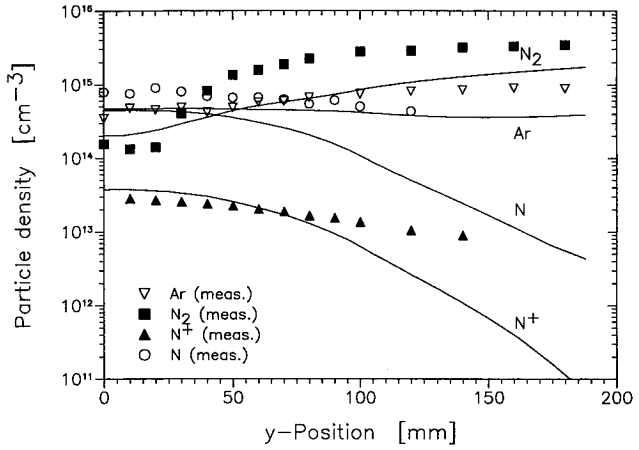

Fig. 17 Comparison of the particle distribution at the second cross section in a N_2/Ar-plasma.

temperature in the center of the jet resulting in a lower dissociation; 2) the lack of source terms concerning excitation due to argon impact (the argon is accounted as molecular nitrogen in the numerical program system up to now); 3) ambient gases outside the plasma jet, which were not taken into account for the numerical simulation but measured by mass spectrometry; and 4) of course, due to systematic errors in the measurement technique by the applied correction factors. Although the data set always contains relatively high errors, the experimental, especially the mass spectrometric data, and the numerical simulation give comparable distributions at the second cross section.

Conclusions

The comparison between the experimental data set, which includes the newly installed mass spectrometric particle distribution, and the numerical simulation with its extended chemical model, yields good qualitative and quantitative agreement. The comparison results in a validation of both the experimental and numerical investigation methods. The newly installed argon chemistry correctly simulates the experimental plasma conditions, i.e., the differences to plasma conditions without using protection gas. It is shown that the effect of the added argon (which is essential for stable arc performance and low anode erosion) on the plasma conditions is measurable, but negligible for material tests. Further investigation will be made concerning the limits of the chemical model used in the numerical simulation and the improvement of measurement accuracy.

Acknowledgments

This work was performed under the auspices of the Sonderforschungsbereich 259 'Hochtemperaturprobleme rückkehrfähiger Raumtransportsysteme' of the Deutsche Forschungsgemeinschaft. We wish to thank our colleague S. Laure for carrying out the pitot and heat flux measurements, and also all colleagues who were involved in the operation of the PWK2.

References

[1]Auweter-Kurtz, M., Habiger, H., Laure, S., Messerschmid, E., Röck, W., and Tubanos, N., "The IRS Plasma Wind Tunnels for the Investigation of Thermal Protection Materials for Reentry Vehicles," 1st European Symposium on Aerothermodynamics for Space Vehicles, ESTEC, Nordwijk, The Netherlands, May 1991.

[2]Schönemann, A., et al., "The Plasma Wind Tunnels PWK1, PWK2," Internal Rept. IRS 92-P6, Inst. für Raumfahrtsysteme, Stuttgart, Germany, July 1992.

[3]Laure, S., Auweter-Kurtz M., Fasoulas, S., Habiger, H., and Röck, W., "The IRS Plasma Wind Tunnels as a Tool for the Investigation of Planetary Entry Missions," AIAA Paper 92-3886, July

1992.

[4]Auweter-Kurtz, M., et al., "Cathode Phenomena in Plasma Thrusters," AIAA Paper 90-2662, July 1990.

[5]Scott, C. D., "Survey of Measurements of Flow Properties in Arcjets," *Journal of Thermophysics and Heat Transfer*, Vol. 7, No. 1, 1993, pp. 9–24.

[6]Willey, R. J., and Blake, D. J., "Gas Composition Measurements in Arc Heated Flowfields via Mass Spectrometry," *Journal of Thermophysics and Heat Transfer*, Vol. 5, No. 2, 1991, pp. 150–156.

[7]Lasgorceix, P., Dudeck, M. A., and Caressa, J. P., "Simulation en Soufflerie de Plasma d'Entrée d'un Vehicle en Region Atmospherique," 1st European Symposium on Aerothermodynamics for Space Vehicles, ESTEC, Nordwijk, The Netherlands, May 1991.

[8]Schönemann, A., and Auweter-Kurtz, M., "Characterization of Nitrogen and Air Plasma Flows by Mass Spectrometry," *ISPC-11, 11th International Symposium on Plasma Chemistry*, Vol. 1, Loughborough, England, UK, 1993, pp. 458–463.

[9]Batey, J. H., "Quadrupole Gas Analysers," *Vacuum*, Vol. 37, No. 8, 1987, pp. 659–668.

[10]Fette, K., and Hesse, J., "Abschätzung der für die Ionenextraktion wichtigen Parameter der Raumladungsschicht," *Zeitschrift für Naturforschung*, Vol. 25A, 1970, pp. 518–524.

[11]Riemann, K.-U., "The Bohm Criterion and Sheath Formation," *Journal of Physics D: Applied Physics*, Vol. 24, 1991, pp. 493–518.

[12]Helm, H., "The Transmission of a Sampling Orifice for Charged and Excited Particles in the Molecular Flow Range," *Plasmaphysik*, Vol. 11, No. 3, 1978, pp. 147–153.

[13]Swift, J. W., and Schawr, M. J. R., *Electrostatic Probes for Plasma Diagnostics*, Ilille Book Ltd., London, 1970.

[14]Habiger, H., Auweter-Kurtz, M., and Kurtz, H., "Electrostatic Probes for the Investigation of Arc-Driven Electric Propulsion Devices," 23rd International Electric Propulsion Conf., IEPC 93-124, Seattle, WA, Sept. 1993.

[15]Chen, S. L., and Sekiguchi, T., "Instantaneous Direct-Display System of Plasma Parameters by Means of Triple-Probe," *Journal of Applied Physics*, Vol. 36, No. 8, 1965, pp. 2363–2375.

[16]Bohn, W. L., Beth, M.-U., and Nedder, G., "On Spectroscopic Measurements of Velocity Profiles and Non-Equilibrium Radial Temperatures in an Argon Plasma Jet," *Journal of Quantum Spectroscopy and Radiative Transfer*, Vol. 7, 1967, pp. 661–676.

[17]Pope, R. B., "Measurements of Enthalpy in Low Density Arc Heated Flows," *AIAA Journal*, Vol. 6, No. 1, 1968, pp. 103–110.

[18]Pope, R. B., "Stagnation Point Convective Heat Transfer in Frozen Boundary Layers," *AIAA Journal*, Vol. 6, No. 4, 1968, pp. 619–626.

[19]Marvin, J. G., and Pope, R. B., "Laminar Convective Heating and Ablation in the Mars Atmosphere," *AIAA Journal*, Vol. 5, No. 2, 1967, pp. 240–248.

[20]Fasoulas, S., Auweter-Kurtz, M., and Habiger, H., "Experimental Investigation of a Nitrogen High Enthalpy Flow," *Journal of Thermophysics and Heat Transfer*, Vol. 8, No. 1, 1993, pp. 48–58.

[21]Fasoulas, S., Auweter-Kurtz, M., Habiger, H., Laure, S., and Sleziona, C., "Investigation of a Nitrogen Flow Within a Plasma Wind Tunnel," AIAA Paper 93-2817, July 1993.

[22]Sleziona, P. C., Auweter-Kurtz, M., Gogel, T., and Messerschmid, E., "Computational Investigation of a Nitrogen Flow in a Plasma Wind Tunnel," AIAA Paper 92-4014, July 1992.

[23]Sleziona, P. C., Gogel, T. H., and Messerschmid, E. W., "Non-Equilibrium Flow in a Hypersonic Expansion Nozzle," Final Rept. for the HERMES R&Q Program, IRS 92-P14/H-ST-1-1134-AMD, Oct. 1992.

[24]Yos, J. M., "Transport Properties of Nitrogen, Hydrogen, Oxygen and Air to 30000K," AVCO Corp., RAD-TM-63-7, 1963.

[25]MacCormack, R. W., "The Effect of Viscosity in Hypersonic Impact Cratering," AIAA Paper 69-354, 1969.

[26]Park, C., *Nonequilibrium Hypersonic Aerothermodynamics*, Wiley, New York, 1990.

[27]Park, C., "Review of Chemical-Kinetic Problems of Future NASA Missions, I: Earth Entries," *Journal of Thermophysics and Heat Transfer*, Vol. 7, No. 3, 1993, pp. 385–398.

[28]Schönemann, A. T., Auweter-Kurtz, M., Habiger, H., Sleziona, P. C., and Stöckle, T., "Experimental and Numerical Investigation of the Influence of Argon Used as Protection Gas in a Reentry Simulation Device," AIAA Paper 93-2829, July 1993.

[29]Gaucherel, P., and Rowe, B., "Measurements of Rates of Charge Exchange and Dissociative Recombination Reactions in Ar-N_2, Ar-H_2 and Ar-O_2 Mixtures," *International Journal of Mass Spectrometry and Ion Physics*, Vol. 25, 1977, pp. 211–227.

[30]Lindinger, W., Howorka, F., Lukac, P., Kuhn, S., Villinger, H., Alge, E., and Ramler, H., "Charge Transfer of $Ar^+ + N_2 \leftrightarrow N_2^+ +$ Ar at Near Thermal Energies," *Physical Review, A*, Vol. 23, 1981, pp. 2319–2326.

[31]Byron, S., "Shock-Tube Measurements of the Rate of Dissociation of Nitrogen," *Journal of Chemical Physics*, Vol. 44, 1966, pp. 1378–1388.

[32]Lindinger, W., Albritton, D. L., McFarland, M., Fehsenfeld, F. C., Schmettekopf, A. L., and Ferguson, E. E., "Rate Constants for the Reactions $O_2^+(a^4\Pi_u)$ Ions with N_2, Ar, CO_2, H_2 and O_2 at Relative Kinetic Energies 0.04-2eV," *Journal of Chemical Physics*, Vol. 62, 1975, pp. 4101–4110.

[33]Kondratiev, V. N., and Nikitin E. E., "Rate Constants for the Process $O_2 + Ar \leftrightarrow O + O + Ar$," *Journal of Chemical Physics*, Vol. 45, 1966, pp. 1078, 1079.

[34]Dotan, I., Fehsenfeld, F. C., and Albritton, D. L., "Rate Constants for the Reactions of Metastable $NO^+(a3^+)$ Ions with SO_2, CO_2, CH_4, N_2, Ar, H_2, D_2 and O_2 at Relative Kinetic Energies 0.04–2.5eV," *Journal of Chemical Physics*, Vol. 71, 1979, pp. 3280–3288.

[35]Warneck, P., "Studies of Ion-Neutral Reactions by a Photoionization Mass-Spectrometer Technique. Charge Transfer Reactions of Argon Ions at Near-Thermal Energies," *Journal of Chemical Physics*, Vol. 46, 1967, pp. 513–519.

[36]Wray, K. L., and Teare, J. D., "Shock-Tube Study of the Kinetics of Nitric Oxide at High Temperatures," *Journal of Chemical Physics*, Vol. 36, 1962, pp. 2582–2596.

[37]Finkelnburg, W., and Maecker, H., "Electrische Bögen und thermisches Plasma," *Handbuch der Physik Bd. XXII, Gasentladungen II*, Springer, Berlin, 1956, pp. 254–369.

[38]Schrade, H. O., Bez, W., Höcker, K. H., and Kaeppeler, H. J., "Zur Theorie der Ohm'schen Heizung vollionisierter Plasmen," *Zeitschrift für Naturforschung*, Bd.15a, 1960, pp. 155–168.

[39]Burhorn, F., "Berechnung und Messung der Wärmeleitfähigkeit von Stickstoff bis 13000K," *Zeitschrift für Physik*, Vol. 155, 1959, pp. 42–58.

[40]Schrade, H. O., and Sleziona, P. C., "Interim Scientific Report for Periodic Covering," IRS, Univ. Stuttgart, Stuttgart, Germany, 1989.